

Influence of exciton-exciton correlations on the polarization characteristics of the polariton amplification in semiconductor microcavities

S. Schumacher, N. H. Kwong, and R. Binder

College of Optical Sciences, University of Arizona, Tucson, Arizona 85721, USA

(Dated: November 4, 2018)

Based on a microscopic many-particle theory we investigate the influence of excitonic correlations on the vectorial polarization state characteristics of the parametric amplification of polaritons in semiconductor microcavities. We study a microcavity with perfect in-plane isotropy. A linear stability analysis of the cavity polariton dynamics shows that in the co-linear (TE-TE or TM-TM) pump-probe polarization state configuration, excitonic correlations diminish the parametric scattering process whereas it is enhanced by excitonic correlations in the cross-linear (TE-TM or TM-TE) configuration. Without any free parameters, our microscopic theory gives a quantitative understanding how many-particle effects can lead to a rotation or change of the outgoing (amplified) probe signal's vectorial polarization state relative to the incoming one's.

PACS numbers: 71.35.-y, 71.36.+c, 42.65.Sf, 42.65.-k

I. INTRODUCTION

In the past decade the parametric amplification of polaritons in planar semiconductor microcavities has been the subject of intense experimental and theoretical research, see, e.g., Refs. 1,2,3,4,5,6 or the reviews given in Refs. 7,8,9. In a typical pump-probe setup in a co-circular polarization configuration the amplification of a weak probe pulse has mainly been attributed to four-wave mixing (FWM) processes mediated by the repulsive Coulomb interaction of the exciton constituent of the polaritons excited on the lower polariton branch (LPB).^{3,4,6,10} For a specific pump in-plane momentum (defining the so-called “magic angle”), energy and momentum conservation is best fulfilled for the FWM processes and thus a pronounced angular dependence of this amplification is observed.^{1,3} Since in the strong coupling regime the LPB is spectrally well below the two-exciton scattering continuum, the influence of excitonic correlations in the scattering processes of polaritons on the LPB is strongly suppressed [compared to the situation in a single quantum well (QW) without the strong coupling to a confined photon cavity mode¹¹]. However, even for co-circular pump-probe excitation these correlations must be considered for a complete understanding of the experimental results.^{5,10,12}

Whereas for co-circular pump-probe excitation only exciton-exciton scattering in the electron-spin triplet channel plays a role, for excitations in other vectorial polarization state configurations, excitonic scattering in the electron-spin singlet channel is also expected to contribute to the amplification mechanism. In the latter case, a change (in the following loosely referred to as ‘rotation’) of the vectorial polarization state of the amplified probe signal compared to the incoming one's can be attributed to this coupling of the two spin subsystems excited with right (+) and left (−) circularly polarized light, respectively.^{13,14,15,16,17,18,19,20,21} However, different effects can overshadow rotations in the vectorial polarization state that are caused by the spin-

dependent many-particle interactions that mediate the amplification process, e.g., a splitting of the TE and TM cavity modes^{22,23} (longitudinal-transverse splitting), or an in-plane anisotropy of the embedded QW or the cavity^{21,24}. Furthermore, for not linearly polarized pump excitation an imbalance in the polariton densities in the two spin subsystems (+ and −) will also lead to a rotation in the vectorial polarization state of the amplified signal.^{17,21} These different mechanisms have previously been investigated^{16,17,18,19,21} based on models describing the effective polariton dynamics in the cavity. In these models that describe the system dynamics at the polariton quasi-particle level, the spin-dependent polariton-polariton scattering matrix elements are included as input parameters for the theory. With a reasonable choice of the parameter set, good agreement with experimental results showing rotations in the probe's vectorial polarization state has been obtained.^{16,18,19,21}

In contrast to these previous studies,^{16,17,18,19,21} we employ a microscopic theory that calculates, from a few material parameters, the scattering matrices driving the polariton amplification in the different vectorial polarization state channels²⁵. No additional assumptions for the effective polariton-polariton interaction are needed, which is directly included in our theory via the frequency dependent and complex exciton-exciton scattering matrices.¹⁰ Our theoretical analysis incorporates: (i) the well-established microscopic many-particle theory for the optically-induced QW polarization dynamics based on the dynamics-controlled truncation (DCT) formalism^{26,27}, and (ii) the self-consistent coupling of this dynamics to the dynamics of the optical fields in the cavity modes^{10,28,29} including all vectorial polarization state channels. The theory consistently includes all coherent third order ($\chi^{(3)}$) nonlinearities and the resulting equations of motion are solved in a self-consistent fashion in the optical fields which includes a certain class of higher-order nonlinearities.^{30,31,32} Correlations involving more than two excitons and those involving incoherent excitons are neglected. These effects are not expected to

qualitatively alter the presented results for the considered coherent exciton densities of $\sim 10^{10} \text{ cm}^{-2}$, especially for excitation well below the exciton resonance.

Based on this theory we introduce a linear stability analysis (LSA) of the cavity polariton dynamics as a general and powerful tool to study the role of spin-dependent polariton-polariton scattering (including time-retarded quantum correlations). For steady-state pump excitation and as long as depletion of the pump from scattering into probe and FWM signals can be neglected, the LSA gives comprehensive information about growth and/or decay (in the following only referred to as ‘growth’) rates for probe and FWM intensities in all vectorial polarization states. The growth rates determine the exponential growth of components in different vectorial polarization states over time, and determine together with the initial conditions the ratio of these components after a given growth duration, uniquely determining the final vectorial polarization state. Although the results are obtained for strict steady-state pump excitation, as discussed below they can to a large extent be carried over to the analysis of pump-probe experiments with finite pulse lengths.¹¹

We use this theory to investigate a microcavity system with perfect in-plane isotropy. As an intrinsic effect that is not caused by structural imperfection, we include a splitting of the TE and TM cavity modes as shown in Fig. 1(a). This way we study a system where all vectorial polarization state rotations of the amplified probe signal can unambiguously be traced back to intrinsic phenomena always present in planar semiconductor microcavities, the TE-TM cavity-mode splitting and the spin-dependent polariton-polariton scattering mediating the amplification.

For this system we analyze results that show how for a linearly polarized pump many-particle correlations and the TE-TM cavity-mode splitting lead to different growth rates of the linearly polarized components (TE, TM) in the probe pulse. This difference can lead to rotation in the vectorial polarization state of the amplified probe compared to the incoming one’s.^{16,17,18,19,21} Starting from the equations governing the cavity-polariton dynamics, we take advantage of our theoretical approach to isolate and discuss the frequency-dependent scattering matrices that give rise to this difference in the vectorial polarization state channels. We show that in the studied regime, close to the amplification threshold, even where the correlation contribution in the spin-singlet channel is weak^{15,20}, these correlations can give rise to an almost complete vectorial polarization state rotation into the ‘‘preferred’’ cross-linear (TE-TM or TM-TE) pump-probe configuration for the pump and outgoing probe pulses. For sufficiently long amplification duration, this result can become virtually independent of the input probe’s vectorial polarization state as long as it contains a small component polarized perpendicular to the linearly polarized pump.

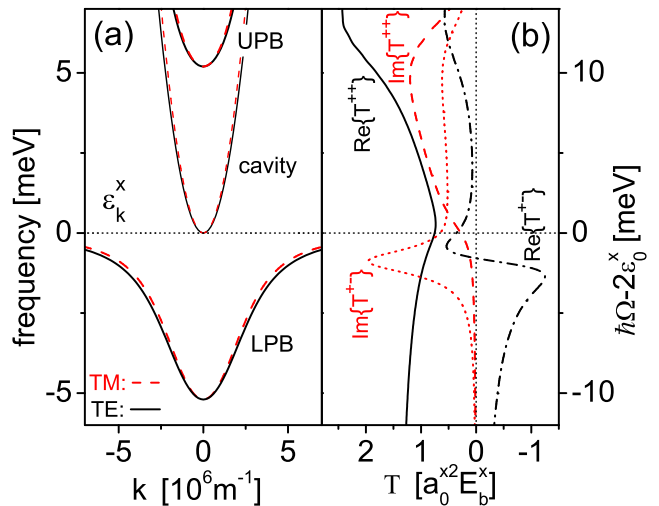


FIG. 1: (color online) (a) Shown is the dependence of the cavity polariton modes on the magnitude k of the in-plane momentum. Depicted are the lower (LPB) and upper (UPB) polariton branches for TE (solid) and TM (dashed) cavity modes, and the bare cavity and exciton (dotted) dispersions. For details on the modeling of the cavity modes see Sec. II. (b) Real and imaginary parts of the two-exciton scattering matrices $\tilde{T}(\Omega)$ in the co-circular ($++$) and counter-circular ($+ -$) polarization state channels. (a,b) Results are shown for typical GaAs parameters³³ as used throughout this work.

II. THE THEORETICAL MODEL

We use a microscopic many-particle theory to describe the coherent QW response to the light field confined in the cavity. Based on the dynamics-controlled truncation (DCT) approach^{26,27} all coherent optically-induced third order nonlinearities, i.e., phase-space-filling (PSF), excitonic mean-field (Hartree-Fock) Coulomb interaction and two-exciton correlations are included on a microscopic level. We use a two-band model (including spin-degenerate conduction and heavy-hole valence band) to describe the optically induced polarization in the GaAs QW.³³ Since we are mainly interested in pump excitation in the LPB, i.e., energetically below the bare exciton resonance (cf. Fig. 1), we account for the dominant contributions to the QW response by evaluating the optically induced QW polarization in the 1s heavy-hole exciton basis.^{29,31,32,34}

We start from the coupled equations of motion for the field $\mathbf{E}_{\mathbf{k}}$ in the cavity modes with in-plane momentum \mathbf{k} (treated in quasi-mode approximation³⁵) and the optically induced interband polarization amplitude $p_{\mathbf{k}}$ in the embedded QW. We formulate our theory in the TE-TM basis for the optical fields in the cavity, $\mathbf{E}_{\mathbf{k}} = E_{\mathbf{k}}^{\text{TE}} \mathbf{e}_{\text{TE}} + E_{\mathbf{k}}^{\text{TM}} \mathbf{e}_{\text{TM}}$ (see Fig. 2 for the excitation geometry), where the field components in the TE mode $E_{\mathbf{k}}^{\text{TE}} \mathbf{e}_{\text{TE}}$ (also called s-polarized) are characterized by an electric field vector with in-plane (in the plane of the

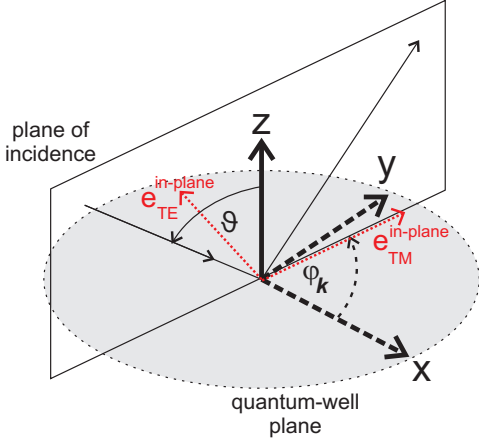


FIG. 2: (color online) Schematic of the excitation geometry. The plane of incidence is spanned by the wave vector of the incoming light field and the z axis. All lines in this plane are solid. The quantum-well plane is the x - y plane. All lines in this plane are broken. The figure shows the basis vectors $\mathbf{e}_{\text{TE}}^{\text{in-plane}}$ and $\mathbf{e}_{\text{TM}}^{\text{in-plane}}$ that span the projection of the TE-TM basis on the x - y plane. The polar angle ϑ and azimuthal angle $\varphi_{\mathbf{k}}$ are also shown. For more explanation see text in Sec. II.

QW) component perpendicular to the in-plane momentum \mathbf{k} , and field components in the TM mode $E_{\mathbf{k}}^{\text{TM}} \mathbf{e}_{\text{TM}}$ (also called p-polarized) by an electric field vector with in-plane component parallel \mathbf{k} . In this basis it is most intuitive to include different cavity-mode exciton couplings for the TE and TM modes in the theory: the in-plane component of the fields in the TE mode does not depend on the polar angle of incidence ϑ (cf. Fig. 2) and thus the coupling strength to the excitonic dipole in the quantum-

well plane does not depend on ϑ . A different result is found for fields in the TM mode where the magnitude of the in-plane component depends on the polar angle of incidence ϑ . Since the z component of fields in the TM mode does not couple to the excitonic dipole for excitation of heavy-hole excitons in the QW³⁶, the effective coupling constant of excitons and fields in the TM mode decreases with the polar angle like $\sim \cos \vartheta$. Additionally, we include a slightly different polar angular dependence of the bare TE and TM cavity dispersions ω_k^{TM} that in general depend on the specific materials and design of the cavity.²² The resulting cavity dispersions are shown in Fig. 1(a) and the parameters will be given later in this section. In order not to complicate the structure of the nonlinear terms in the equations of motion for the polarization amplitudes, we use the usual Cartesian basis (X - Y basis) in the QW plane (x - y plane) to decompose the polarization into its components as $\mathbf{p}_{\mathbf{k}} = p_{\mathbf{k}}^x \mathbf{e}_x + p_{\mathbf{k}}^y \mathbf{e}_y$. In the X - Y basis, the projection of the TE-TM basis vectors on the x - y plane, $\mathbf{e}_{\text{TE}}^{\text{in-plane}}$ and $\mathbf{e}_{\text{TM}}^{\text{in-plane}}$, rotates with the in-plane component \mathbf{k} of the momentum of the incident wave. The azimuthal angle between \mathbf{k} and the x axis is denoted by $\varphi_{\mathbf{k}}$ (cf. Fig. 2). Simple geometric considerations lead to the azimuthal angular dependencies that appear in the terms coupling the equations of motion for field and polarization amplitude components in the different bases:

$$i\hbar \dot{E}_{\mathbf{k}}^{\text{TE}} = \left(\hbar\omega_k^{\text{TM}} - i\gamma_c \right) E_{\mathbf{k}}^{\text{TE}} - V_k^{\text{TM}} \left[p_{\mathbf{k}}^x \cos \varphi_{\mathbf{k}} \pm p_{\mathbf{k}}^y \sin \varphi_{\mathbf{k}} \right] + i\hbar t_c E_{\mathbf{k},\text{inc}}^{\text{TM}}, \quad (1)$$

$$\begin{aligned} i\hbar \dot{p}_{\mathbf{k}}^x &= \left(\hbar\omega_k^x - i\gamma_x \right) p_{\mathbf{k}}^x - \left(V_k^{\text{TM}} E_{\mathbf{k}}^{\text{TE}} \cos \varphi_{\mathbf{k}} \mp V_k^{\text{TE}} E_{\mathbf{k}}^{\text{TM}} \sin \varphi_{\mathbf{k}} \right) \\ &+ \tilde{A} \sum_{\mathbf{k}'\mathbf{k}''} \left(p_{\mathbf{k}'+\mathbf{k}''-\mathbf{k}}^{x*} p_{\mathbf{k}'}^x + p_{\mathbf{k}'+\mathbf{k}''-\mathbf{k}}^{y*} p_{\mathbf{k}'}^y \right) \left(V_{k''}^{\text{TM}} E_{\mathbf{k}''}^{\text{TE}} \cos \varphi_{\mathbf{k}''} \mp V_{k''}^{\text{TE}} E_{\mathbf{k}''}^{\text{TM}} \sin \varphi_{\mathbf{k}''} \right) \\ &+ \tilde{A} \sum_{\mathbf{k}'\mathbf{k}''} \left(p_{\mathbf{k}'+\mathbf{k}''-\mathbf{k}}^{y*} p_{\mathbf{k}'}^x - p_{\mathbf{k}'+\mathbf{k}''-\mathbf{k}}^{x*} p_{\mathbf{k}'}^y \right) \left(V_{k''}^{\text{TE}} E_{\mathbf{k}''}^{\text{TE}} \cos \varphi_{\mathbf{k}''} \pm V_{k''}^{\text{TM}} E_{\mathbf{k}''}^{\text{TM}} \sin \varphi_{\mathbf{k}''} \right) \\ &+ \frac{1}{2} \sum_{\mathbf{k}'\mathbf{k}''} p_{\mathbf{k}'+\mathbf{k}''-\mathbf{k}}^{x*} \int_{-\infty}^{\infty} dt' \left[\left(\mathcal{T}^{++}(t-t') + \mathcal{T}^{+-}(t-t') \right) p_{\mathbf{k}'}^x(t') p_{\mathbf{k}''}^x(t') - \left(\mathcal{T}^{++}(t-t') - \mathcal{T}^{+-}(t-t') \right) p_{\mathbf{k}'}^y(t') p_{\mathbf{k}''}^y(t') \right] \\ &+ \sum_{\mathbf{k}'\mathbf{k}''} p_{\mathbf{k}'+\mathbf{k}''-\mathbf{k}}^{y*} \int_{-\infty}^{\infty} dt' \left[\mathcal{T}^{++}(t-t') p_{\mathbf{k}'}^x(t') p_{\mathbf{k}''}^y(t') \right]. \end{aligned} \quad (2)$$

These equations constitute the generalization of the equations given in Ref. 10, now including all vectorial polarization states. As discussed above, the polarization amplitudes are given in the X - Y basis, while the fields are given in the TE-TM basis.³⁷ The meaning of the symbols in Eq. (2) are to be discussed in the remain-

der of this paragraph, along with the used parameters and approximations. Unless otherwise noted, the time argument in Eqs. (1) and (2) is t . t_c is the coupling constant of the cavity mode to the external light fields $E_{\mathbf{k},\text{inc}}^{\text{TM}}$, and the dephasing constant γ_c describes optical losses from the cavity to the outside world.¹⁰ The depen-

dence of the bare cavity modes ω_k^{TM} and the dependence of the exciton-cavity mode coupling V_k^{TM} on the polar angle ϑ is modeled on a phenomenological level along the guidelines given in Ref. 22. We approximate the bare cavity dispersions with $\omega_k^{\text{TM}} = \frac{\omega_0}{\cos \vartheta} + 100 \text{ meV} \cdot \sin^2 \vartheta$ and $\omega_k^{\text{TE}} = \frac{\omega_0}{\cos \vartheta}$ with $\sin \vartheta = \frac{|\mathbf{k}|c_0}{\omega n_{\text{bg}}}$. This way a TE-TM cavity-mode splitting from the mismatch of the center of the stopband of the cavity mirrors and the Fabry-Perot frequency of the cavity is phenomenologically included.²² The cavity-mode exciton couplings are $V_k^{\text{TM}} = V_0^{\text{TM}} \cos \vartheta$ and $V_k^{\text{TE}} = V_0^{\text{TE}}$, respectively, with $V_0^{\text{TM}} = V_0^{\text{TE}} = 5.2 \text{ meV}$. With $\hbar\omega_0^{\text{TM}} = \varepsilon_0^x$ we assume zero cavity-mode exciton splitting for $k = 0$. The chosen parameters³³ give a reasonable magnitude and polar angular dependence of the TE-TM mode splitting in the LPB, comparable to the results in, e.g., Ref. 23. Since the presented results do not crucially depend on the details of the cavity-mode splitting, no further insight is expected from a more elaborate treatment. In Eq. (2), $\hbar\omega_k^x$ is the 1s heavy-hole exciton in-plane dispersion, γ_x a phenomenological dephasing constant of the excitonic polarization amplitude, and \tilde{A} is related to the excitonic PSF constant A^{PSF} by $\tilde{A} = \frac{A^{\text{PSF}}}{\phi_{1s}^*(\mathbf{0})}$, with $\phi_{1s}(\mathbf{r})$ being the two-dimensional QW exciton wavefunction. Without loss of generality, in the following the quantities ϕ_{1s} , V_0^{TM} , and t_c are chosen to be real-valued. The parameter values are listed in Ref. 33. Although in this paper we investigate a spatially isotropic microcavity-system, spatial anisotropy can easily be included in the theory via $\omega_k^x \rightarrow \omega_{\mathbf{k}}^x$ to model an anisotropic dispersion of the QW excitons and via $\omega_k^{\text{TM}} \rightarrow \omega_{\mathbf{k}}^{\text{TM}}$ to model anisotropy of the cavity modes. The two-exciton scattering matrices (T-matrices) \mathcal{T} in the co-circular ($++$) and counter-circular ($+ -$) polarization state channels include a two-exciton dephasing rate 2γ and are given by $\mathcal{T}^{++} = \mathcal{T}^+$ and $\mathcal{T}^{+-} = (\mathcal{T}^+ + \mathcal{T}^-)/2$, with the T-matrices \mathcal{T}^+ and \mathcal{T}^- in the electron-spin triplet and singlet channel, respectively, as defined in Eq. (32) of Ref. 25. The frequency dependence of real and imaginary parts of \mathcal{T}^{++} and \mathcal{T}^{+-} is shown in Fig. 1(b). We neglect the momentum dependence of the T-matrices for scattering processes involving two excitons with different in-plane momenta. Calculations in a different context have shown that this is justified in a good approximation for the small optical momenta contributing here.³⁸ We also neglect possible corrections to the excitonic T-matrices from the coupling to the photons in the cavity modes. This is supported by experimental observations that indicate that even in the strong coupling regime the biexciton binding energy is not significantly affected by the coupling to the cavity modes.³⁹ Also, good theory-experiment agreement has been achieved in Refs. 28,29,40 using a theory based on pure exciton-exciton scattering matrices.

To simulate a typical pump-probe setup, we start from Eqs. (1) and (2) and chose a finite in-plane momentum \mathbf{k}_p for the pump propagating along a given axis, here,

without loss of generality the x axis, i.e., $\varphi_{\mathbf{k}_p} = 0$. We “detect” the probe in normal incidence with in-plane momentum $\mathbf{k} = 0$ where in the past the strongest amplification has been observed.^{10,12,16,41} This fixes the in-plane momentum of the background-free FWM signal to $2\mathbf{k}_p$. We go beyond an evaluation of the theory on a strict $\chi^{(3)}$ level by self-consistently calculating the resulting excitonic and biexcitonic polarization amplitude dynamics up to arbitrary order in the pump field^{30,31} and we linearize the equations of motion in the weak probe field. Only via this self-consistent solution the coupling of the probe signal to the background-free FWM signal is included in the theory which provides the basic feedback mechanism that leads to the unstable behavior in, e.g., Refs. 1,2,3,4,5,7,8. We limit our analysis to coherent exciton densities that are low enough [$\lesssim 2 \times 10^{10} \text{ cm}^{-2}$, cf. Figs. 3 and 4] so that neglect of higher than two-exciton Coulomb correlations can be justified.

III. LINEAR STABILITY ANALYSIS

In this section we introduce the linear stability analysis (LSA) used in the remainder of this paper. To analyze the stability of the pump-probe dynamics the LSA is done without an incoming probe field and for a linearly polarized monochromatic continuous wave (cw) pump field $E_{\mathbf{k}_p}^{\text{TM}}(t) = \tilde{E}_{\mathbf{k}_p}^{\text{TM}}(\omega_p)e^{-i\omega_p t}$ inducing the pump polarization amplitude $p_{\mathbf{k}_p}^x(t) = \tilde{p}_{\mathbf{k}_p}^x(\omega_p)e^{-i\omega_p t}$, with $\dot{\tilde{p}}_{\mathbf{k}_p}^x = 0$ and $\dot{\tilde{E}}_{\mathbf{k}_p}^{\text{TM}} = 0$ (ω_p is the pump frequency). The pump polarization amplitude is a solution of the cubic nonlinear pump equation following from Eqs. (1) and (2) for unidirectional light propagation and is determined as outlined in Appendix A. The resulting coherent exciton density $|p_{\mathbf{k}_p}^x|^2$ for excitation with a linearly polarized pump of fixed intensity is shown in Figs. 3 and 4 as a function of the magnitude of the pump in-plane momentum $|\mathbf{k}_p|$ and pump detuning $\Delta\varepsilon$ from the bare exciton resonance for excitation in the TE or TM mode, respectively. No bistable behavior of the pump-induced exciton density in Figs. 3 and 4 is found (this follows from the solution of the nonlinear pump equation as outlined in Appendix A). However, for other values of cavity or QW parameters and a different pump intensity, bistability may occur, which would complicate our discussion^{41,42}. The pump densities shown have their maxima close to the linear polariton dispersions (included as the dashed lines) and decrease along the LPB with increasing in-plane momentum because of the decreased coupling of the (mostly exciton-like) large-momentum polariton states to the incoming field. Furthermore, a reduced exciton density is found for excitation of the UPB caused by strong excitation-induced dephasing (EID) for pump excitation in the two-exciton scattering continuum (the spectral region where the two-exciton scattering matrices shown in Fig. 1 exhibit a large imaginary part). For the stability

analysis we evaluate the memory integrals in Eq. (2) contributing to the probe and FWM directions in a Markov approximation for the two-exciton scattering continua in the T-matrices \mathcal{T}^{++} and \mathcal{T}^{+-} . Our Markov approximation is effected by taking $p_0(t') \approx p_0(t)e^{i\omega_p(t-t')}$ and $p_{2k_p}(t') \approx p_{2k_p}(t)e^{i\omega_p(t-t')}$ where the probe and FWM polarization amplitudes p_0 and p_{2k_p} appear under the time-retarded integrals in Eq. (2) together with the continuum contributions in \mathcal{T}^{++} and \mathcal{T}^{+-} . In contrast, we include the bound biexciton state exactly via the time-dependent amplitudes $b_{\mathbf{k}_p}(t)$ and $b_{3\mathbf{k}_p}(t)$. For this we separate the bound biexciton contributions \mathcal{T}_{xx}^{+-} from the correlation kernels \mathcal{T}^{+-} in Eq. (2) as $\mathcal{T}^{+-} = \mathcal{T}_{\text{cont}}^{+-} + \mathcal{T}_{xx}^{+-}$. The bound biexciton contributions to Eq. (2) can be exactly included via the equations of motion [cf. Eqs. (11) and (12) of Ref. 25] for the biexciton amplitudes $b_{\mathbf{k}_p}(t)$ and $b_{3\mathbf{k}_p}(t)$ which are labeled according to the total in-plane momentum of their source terms: $\sim p_0 p_{\mathbf{k}_p}$ and $\sim p_{2\mathbf{k}_p} p_{\mathbf{k}_p}$, respectively. This way we include quantum memory effects related to the excitation of bound biexcitons, which were previously shown to play an important role in the study of FWM instabilities in single semiconductor QWs¹¹. Since, for the chosen excitation geometry with finite pump in-plane momentum \mathbf{k}_p , the probe and FWM signals do not oscillate at the pump frequency ω_p , the Markov approximation for the two-exciton scattering continuum may not be as justified as it is for the single QW system investigated in Ref. 11. However, close to or in the unstable regime, those wave mixing processes that describe the pairwise scattering of pump polaritons into the probe and FWM directions play the dominant role in the probe and FWM dynamics. For monochromatic cw pump excitation these terms are of purely Markovian nature and hence the T-matrices in these terms contribute exactly at frequency $\Omega = 2\omega_p$; no approximation is required. And indeed, for the results discussed here, not even from the excitation of the bound biexciton state have we found a sizable contribution from non-Markovian (quantum memory) effects. For monochromatic cw pump excitation and with the ansatz $E_0^{\text{TE}}(t) = \tilde{E}_0^{\text{TE}}(t)e^{-i\omega_p t}$, $E_{2\mathbf{k}_p}^{\text{TE}}(t) = \tilde{E}_{2\mathbf{k}_p}^{\text{TE}}(t)e^{-i\omega_p t}$, $p_0^{\text{X}}(t) = \tilde{p}_0^{\text{X}}(t)e^{-i\omega_p t}$, $p_{2\mathbf{k}_p}^{\text{X}}(t) = \tilde{p}_{2\mathbf{k}_p}^{\text{X}}(t)e^{-i\omega_p t}$ and $b_{\mathbf{k}_p}(t) = \tilde{b}_{\mathbf{k}_p}(t)e^{-i2\omega_p t}$, $b_{3\mathbf{k}_p}(t) = \tilde{b}_{3\mathbf{k}_p}(t)e^{-i2\omega_p t}$ the coupled probe and FWM dynamics can be written in the form

$$\hbar\dot{\tilde{p}}(t) = M\tilde{p}(t). \quad (3)$$

The vector

$$\tilde{p}(t) = [\tilde{E}_0^{\text{TE}}(t), \tilde{E}_{2\mathbf{k}_p}^{\text{TE}*}(t), \tilde{E}_0^{\text{TM}}(t), \tilde{E}_{2\mathbf{k}_p}^{\text{TM}*}(t), \tilde{p}_0^{\text{Y}}(t), \tilde{p}_{2\mathbf{k}_p}^{\text{Y}*}(t), \tilde{p}_0^{\text{X}}(t), \tilde{p}_{2\mathbf{k}_p}^{\text{X}*}(t), \tilde{b}_{\mathbf{k}_p}(t), \tilde{b}_{3\mathbf{k}_p}^*(t)]^T,$$

groups field and polarization amplitude variables together. M is a time-independent matrix where all system parameters and the steady-state pump polarization amplitude (Figs. 3 and 4) and the corresponding pump field in the cavity modes parametrically enter the analysis. For excitation with a linearly polarized pump either exciting the TE or the TM mode, the matrix M is block-diagonal for the components of probe and FWM parallel (co-linear configuration) and perpendicular (cross-linear configuration) to the pump's vectorial polarization state. Then for each pump polarization state (TE or TM, respectively), the 10×10 matrix M can be decomposed into the 6×6 block $M_{\parallel}^{\sigma_s, \sigma_p}$ with $\sigma_s = \sigma_p$ and the 4×4 block $M_{\perp}^{\sigma_s, \sigma_p}$ with $\sigma_s \neq \sigma_p$ which describe the dynamics of the coupled variables in the vectors $\tilde{p}_{\parallel}^{\sigma_s}(t) = [\tilde{E}_0^{\sigma_s}(t), \tilde{E}_{2\mathbf{k}_p}^{\sigma_s*}(t), \tilde{p}_0^{\sigma_s}(t), \tilde{p}_{2\mathbf{k}_p}^{\sigma_s*}(t), \tilde{b}_{\mathbf{k}_p}(t), \tilde{b}_{3\mathbf{k}_p}^*(t)]^T$ with $\sigma_s = \sigma_p$ for the co-linear configurations and $\tilde{p}_{\perp}^{\sigma_s}(t) = [\tilde{E}_0^{\sigma_s}(t), \tilde{E}_{2\mathbf{k}_p}^{\sigma_s*}(t), \tilde{p}_0^{\sigma_s}(t), \tilde{p}_{2\mathbf{k}_p}^{\sigma_s*}(t)]^T$ with $\sigma_s \neq \sigma_p$ for the cross-linear configurations, respectively. The indices σ_s and σ_p relate to the cavity modes TE and TM, or to the corresponding excitonic polarization amplitude components X and Y that are excited by the fields in these modes. Note, that for the above-described excitation situation (pump pulse propagating along the x axis and linearly polarized excitation in TE or TM mode) the x component of the polarization amplitude is exclusively excited by fields in the TM mode and the y component by fields in the TE mode. The matrices $M_{\parallel}^{\sigma_s, \sigma_p}$ and $M_{\perp}^{\sigma_s, \sigma_p}$ can be derived from Eqs. (1) and (2) and take the following form:

$$M_{\perp}^{\sigma_s, \sigma_p} = \begin{pmatrix} h_0^{\sigma_s} & 0 & iV_0^{\sigma_s} & 0 \\ 0 & h_{2k_p}^{\sigma_s*} & 0 & \frac{1}{i}V_{2k_p}^{\sigma_s*} \\ V_{0,\text{eff}}^{\sigma_s, \sigma_p} & 0 & a_{0,\perp}^{\sigma_p} & b_{\perp}^{\sigma_p} \\ 0 & V_{2k_p,\text{eff}}^{\sigma_s, \sigma_p*} & b_{\perp}^{\sigma_p*} & a_{2k_p,\perp}^{\sigma_p*} \end{pmatrix}, \quad (4)$$

$$M_{\parallel}^{\sigma_s, \sigma_p} = \begin{pmatrix} h_0^{\sigma_s} & 0 & iV_0^{\sigma_s} & 0 & 0 & 0 \\ 0 & h_{2k_p}^{\sigma_s*} & 0 & \frac{1}{i}V_{2k_p}^{\sigma_s*} & 0 & 0 \\ V_{0,\text{eff}}^{\sigma_s, \sigma_p} & 0 & a_{0,\parallel}^{\sigma_p} & b_{\parallel}^{\sigma_p} & C\sigma_p & 0 \\ 0 & V_{2k_p,\text{eff}}^{\sigma_s, \sigma_p*} & b_{\parallel}^{\sigma_p*} & a_{2k_p,\parallel}^{\sigma_p*} & 0 & C\sigma_p^* \\ 0 & 0 & -\frac{1}{2}C\sigma_p^* & 0 & B_{0,k_p} & 0 \\ 0 & 0 & 0 & -\frac{1}{2}C\sigma_p & 0 & B_{k_p,2k_p}^* \end{pmatrix}. \quad (5)$$

The time-independent coefficients are defined as:

$$h_k^{\sigma_s} = \frac{1}{i}(\hbar\omega_k^{\sigma_s} - \hbar\omega_p - i\gamma_c),$$

$$V_{k,\text{eff}}^{\sigma_s,\sigma_p} = iV_k^{\sigma_s} \left(1 - \tilde{A}|\tilde{p}_{\mathbf{k}_p}^{\sigma_p}|^2\right),$$

$$a_{k,i}^{\sigma_p} = \frac{1}{i} \left[-\Delta\varepsilon_k - i\gamma_x + \tilde{A}V_{k_p}^{\sigma_p} \tilde{p}_{\mathbf{k}_p}^{\sigma_p*} \tilde{E}_{\mathbf{k}_p}^{\sigma_p} + (\tilde{\mathcal{T}}^{++}(2\omega_p) + \delta_{i,\parallel} \tilde{\mathcal{T}}_{\text{cont}}^{+-}(2\omega_p)) |\tilde{p}_{\mathbf{k}_p}^{\sigma_p}|^2 \right],$$

$$b_i^{\sigma_p} = \frac{1}{i} \left[(-1)^{\delta_{i,\perp}} \tilde{A}V_{k_p}^{\sigma_p} \tilde{p}_{\mathbf{k}_p}^{\sigma_p} \tilde{E}_{\mathbf{k}_p}^{\sigma_p} + \frac{1}{2} \left((-1)^{\delta_{i,\perp}} \tilde{\mathcal{T}}^{++}(2\omega_p) + \tilde{\mathcal{T}}^{+-}(2\omega_p) \right) \tilde{p}_{\mathbf{k}_p}^{\sigma_p 2} \right],$$

$$B_{k_1,k_2} = \frac{1}{i} (-\Delta\varepsilon_{k_1} - \Delta\varepsilon_{k_2} - 2i\gamma_x - E_b^{xx}),$$

$$C^{\sigma_p} = \frac{1}{i} (C_{xx} \tilde{p}_{\mathbf{k}_p}^{\sigma_p*}),$$

$$C_{xx} = \left(\left[\sum_{\mathbf{q}} W_{xx}^{-\dagger}(\mathbf{q}, 0) \zeta(\mathbf{q}) \right] \left[\sum_{\mathbf{q}'} \zeta^\dagger(\mathbf{q}') W_{xx}^-(\mathbf{q}', 0) \right] \right)^{\frac{1}{2}}.$$

$\tilde{\mathcal{T}}^{++}(\Omega)$ and $\tilde{\mathcal{T}}^{+-}(\Omega)$ are the Fourier transformed correlation kernels as shown in Fig. 1(b) and defined by Eqs. (27) and (32) of Ref. 25. The coupling strength $C_{xx} \approx 0.54 E_b^x a_0^x$ of the excitonic polarization amplitudes to the bound biexciton amplitude is given by the biexciton ground state wave function $\zeta(\mathbf{q})$ in the electron spin singlet configuration and the corresponding two-exciton Coulomb interaction matrix element $W_{xx}^-(\mathbf{q}, 0)$, both as defined in Eqs. (14) and (24) of Ref. 25.

For steady-state monochromatic pump excitation, the linear stability analysis formulated in this section gives us comprehensive information about growth (real-part of the eigenvalues of M) and frequency (imaginary-part of the eigenvalues of M) of the polariton modes in the probe and FWM directions, after the initial external driving pulse (seed) in the probe direction is gone. Information how the different eigenmodes contribute to the polarization amplitudes and fields with different in-plane momenta (0 or $2\mathbf{k}_p$) can be obtained from the eigenvectors of the matrices M . If at least one of the eigenvalues λ_i of the matrices M fulfills $\text{Re}\{\lambda_i\} > 0$, the system is unstable. An arbitrarily small seed of p_0^X or $p_{2\mathbf{k}_p}^Y$ (X or Y, depending on which subspace shows an unstable dynamics) or in the corresponding cavity modes would grow exponentially until the matrix M ceases to describe the system correctly.

In addition to the strict steady-state analysis (regarding the pump excitation), the general information obtained from the stability analysis can – to a large extent

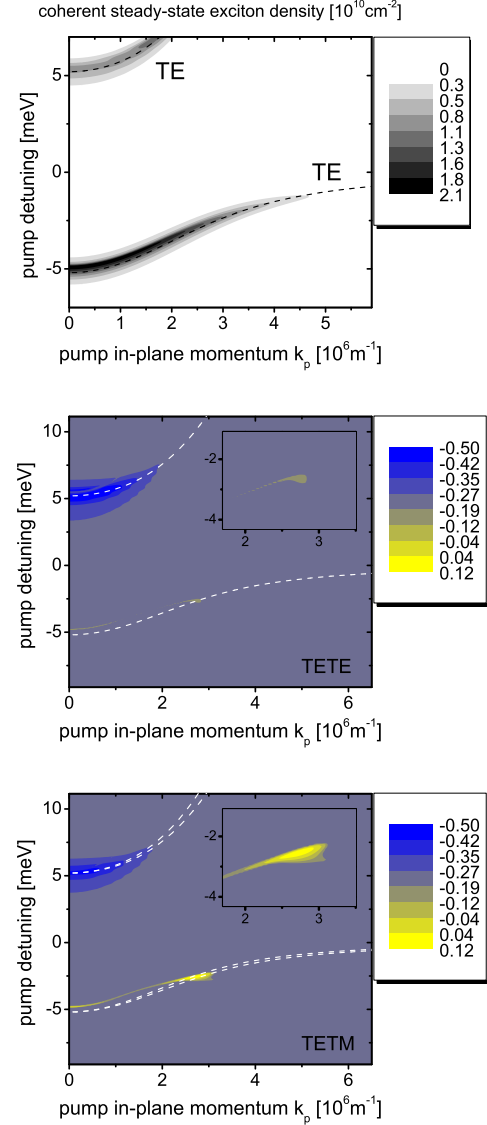


FIG. 3: (color online) Top: Coherent steady-state exciton density $|p_{k_p}^Y|^2$ for a fixed pump intensity of a linearly TE polarized pump as a function of the magnitude k_p of the pump in-plane momentum and the pump detuning $\Delta\varepsilon = \hbar\omega_p - \varepsilon_0^x$ from the bare exciton resonance ε_0^x . The linear polariton dispersions are included as the dashed lines. Middle and lower figures show the real part of the eigenvalue of $M_{\parallel}^{\text{TE,TE}}$ and $M_{\perp}^{\text{TE,TM}}$ with the largest real part in meV (maximum growth rate if larger than zero). The linear polariton dispersions are included as the dashed lines and the insets show the same data around the “magic angle” for pump excitation on the LPB.

– be carried over to the discussion of pump-probe experiments with finite pulse lengths. From the linear stability analysis reasonable predictions for growth rates of probe and FWM signals and thus for polarization rotations can be made as long as no external probe pulse significantly drives the probe polariton dynamics during the period of

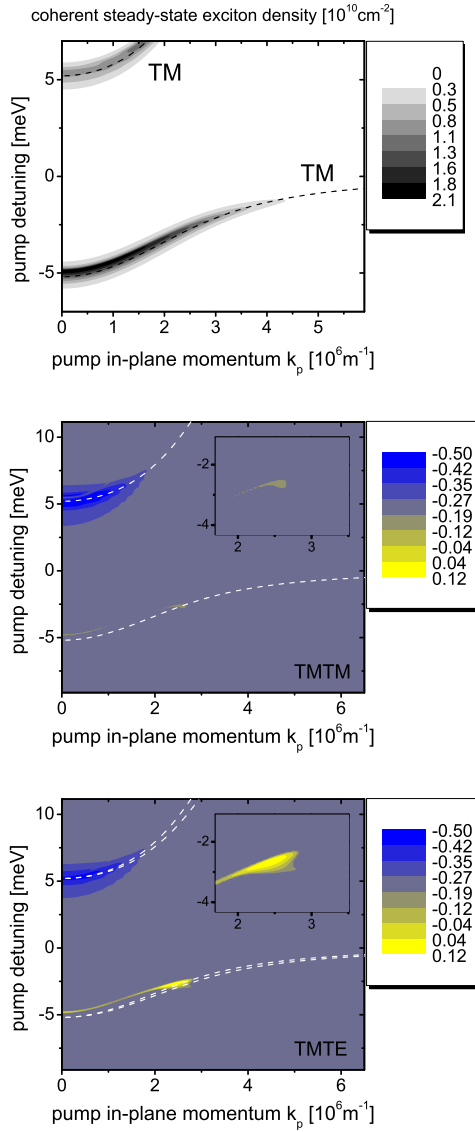


FIG. 4: (color online) Same as Fig. 3 but for linearly TM polarized pump.

amplification. Furthermore, for interpretation of pulsed experiments based on the linear stability analysis, the pump pulse must be spectrally sufficiently narrow and pump and probe must have significant temporal overlap. After a sufficiently long period of time that particular eigenmode of M corresponding to the eigenvalue with the largest real part will dominate the overall outgoing signal in probe and FWM directions. In a pump-probe experiment an incoming probe pulse in this particular mode will be most efficiently amplified, or for steady-state pump excitation without an incoming probe, fluctuations in this mode (serving as a seed) will grow most efficiently over time and dominate the signal in probe and FWM direction after a sufficiently long growth period.

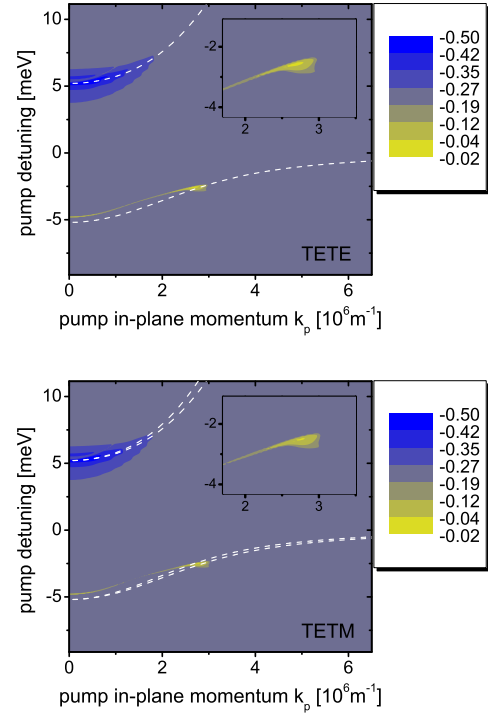


FIG. 5: (color online) Same as the two lower panels in Fig. 3 but without exciton-exciton scattering in the $+-$ channel ($\tilde{\mathcal{T}}^{+-} \equiv 0$).

IV. RESULTS AND DISCUSSION

Without excitonic correlations (and neglecting the TE-TM-splitting of the cavity modes) the equations of motion for the two circular polarization state channels, $+$ and $-$, are decoupled. In this case, for excitation with a linearly polarized pump, where equal densities of polaritons are excited in these two different polarization state channels, the incoming (seed in our linear stability analysis) and outgoing probe are always in the same vectorial polarization state, in the stable (all $\text{Re}\{\lambda\} < 0$) as well as in the unstable (at least one $\text{Re}\{\lambda\} > 0$) regime. Neglecting the TE-TM cavity-mode splitting, for the pump in a linear polarization state, only the spin-dependent excitonic correlations can give rise to a rotation of the outgoing probe signal's vectorial polarization state relative to the incoming one's. The actual fraction of polaritons that is scattered into the probe and FWM directions in a vectorial polarization state perpendicular or parallel to the pump's vectorial polarization state, respectively, strongly depends on the excitonic correlations in the $+-$ polarization state channel (included in \mathcal{T}^{+-}).⁹ As discussed in the previous section, for a linearly polarized (either TE or TM) pump, all the eigenmodes [eigenvectors of the matrix M in Eq. (3)] for the probe and FWM dynamics are either polarized parallel (co-linear configuration) or perpendicular (cross-linear configuration) to the pump, even when both excitonic correlations and cavity-mode split-

ting are included. However, either excitonic correlations alone or the cavity-mode splitting alone (when the polariton scattering is mediated by Hartree-Fock Coulomb interaction) is sufficient to give different probe and FWM dynamics in the two different polarization state configurations.

Since the above-listed effects lead to a difference in the growth rates of the modes polarized parallel or perpendicular to the pump, for an arbitrarily polarized probe the two different vectorial polarization state components (parallel or perpendicular) will grow differently over time. The stronger the amplification of the probe and the longer the amplification duration, the more the fractions of the probe in those modes that exhibit the fastest exponential growth, will dominate the outgoing probe and FWM signals. Thus, for strong amplification, the growth rates of the fastest growing modes in the two polarization states (parallel and perpendicular) ultimately determine the rotation in the probe's vectorial polarization state. Studying these growth rates also answers the question about the preferred mode for the growth of probe fluctuations over time, when no incoming probe is present. Figures 3 and 4 show these growth rates – the real part of the eigenvalue of M with the largest real part in each case – for a fixed pump intensity for the different polarization state configurations (co-linear or cross-linear) for pump excitation of TE (Fig. 3) and TM (Fig. 4) mode, respectively. The results show that pumping either TE or TM mode does not significantly influence the overall result regarding the maximum growth rates in the co-linear or cross-linear configuration; merely a small change in the optimum pump momentum and frequency is observed. However, a significant difference between co-linear and cross-linear configuration is found for pumping close to the inflection point of the LPB (the so-called “magic angle”) where phase-matching is best fulfilled so that triply-resonant (resonant for the pump excitation and at an angle so that the dispersions in probe and FWM directions allow for phase-matched scattering of pairs of pump-excited polaritons into these two directions) amplification of the polaritons can occur. For the chosen intensity, close to the instability threshold, and for pump excitation under the “magic angle” we are in a regime where instability ($\text{Re}\{\lambda\} > 0$) and corresponding exponential signal growth is only found in the cross-linear configurations (TE-TM and TM-TE) while all the modes in the co-linear configurations (TE-TE and TM-TM) are exponentially decaying. In this regime, for an arbitrarily polarized probe, only that component polarized perpendicular to the pump is exponentially growing over time and thus only this component experiences significant amplification. To isolate the mechanism that leads to this striking difference in the polarization state configurations, Fig. 5 shows results for both configurations in Fig. 3 but without taking into account the correlations in the $+ -$ channel ($\tilde{\mathcal{T}}^{+-} \equiv 0$). Without these correlations the results for the two configurations almost look alike; we find only a small difference in the growth

rates caused by the TE-TM cavity-mode splitting. Note that without the correlations in the $+ -$ channel in both configurations the instability threshold is not reached for the same pump intensity as used in Figs. 3 and 4.

In the co-circular ($++$) excitation configuration it was found earlier¹⁰ that excitonic correlations in the $++$ channel may considerably reduce the maximum growth rates in the polariton amplification. In the $++$ channel the driving mechanism for the instabilities, the phase-conjugate feedback, is weakened by the two-exciton correlations. Additionally, but for large negative detuning less important, correlations in the $++$ channel give rise to pump-induced EID, also reducing the exponential growth rate over time. Figures 3 and 4 show that the correlations in the $+ -$ channel enhance the growth rate in the cross-linear configuration and diminish it in the co-linear configuration, compared to the results shown in Fig. 5 where these correlations are absent.

In the following we will interpret these results in terms of the exciton-exciton scattering matrices shown in Fig. 1(b) for the different polarization state channels of polariton-polariton scattering. For this discussion we ignore the small PSF nonlinearities that contribute to the probe and FWM dynamics, and concentrate on the nonlinearities in the excitonic polarization amplitudes in Eq. (2) that contribute to the probe and FWM dynamics and therefore determine the amplification process. Being sufficient for a qualitative understanding we discuss all contributions in Markov approximation. Three different terms have to be analyzed that enter the matrices M in Eqs. (4) and (5):

(i) Excitation-induced dephasing for the excitonic component of the polaritons (entering M via $a_{k,i}^{\sigma_p}$):

$$\text{Im}\left\{\tilde{\mathcal{T}}^{++}(2\omega_p) + \delta_{i,\parallel}\tilde{\mathcal{T}}^{+-}(2\omega_p)\right\}|\tilde{p}_{\mathbf{k}}^{\sigma_p}|^2. \quad (6)$$

(ii) Nonlinear shifts to the effective exciton resonances in probe and FWM direction (entering M via $a_{k,i}^{\sigma_p}$):

$$\text{Re}\left\{\tilde{\mathcal{T}}^{++}(2\omega_p) + \delta_{i,\parallel}\tilde{\mathcal{T}}^{+-}(2\omega_p)\right\}|\tilde{p}_{\mathbf{k}}^{\sigma_p}|^2. \quad (7)$$

(iii) The phase-conjugate oscillation feedback for the excitonic constituents of the polaritons that drives the instability (entering M via $b_i^{\sigma_p}$):

$$\frac{1}{2}\left((-1)^{\delta_{i,\perp}}\tilde{\mathcal{T}}^{++}(2\omega_p) + \tilde{\mathcal{T}}^{+-}(2\omega_p)\right)\tilde{p}_{\mathbf{k}}^{\sigma_p^2}. \quad (8)$$

The index $i \in \{\perp, \parallel\}$ labels the co- and cross-linear polarization state configurations, respectively. The maximum growth rates in Figs. 3 to 5 are obtained when the pump is tuned about 3 meV below the exciton resonance and close to the “magic angle”. For this pump detuning and in Markov approximation the two-exciton scattering matrices shown in Fig. 1(b) contribute at $\hbar\Omega - 2\varepsilon_x \approx -6$ meV. For this detuning the $\text{Im}\{\tilde{\mathcal{T}}^{++}\}$ is much smaller than $\text{Im}\{\tilde{\mathcal{T}}^{+-}\}$ which according to Eq. (6) leads to a much larger EID in the co-linear (\parallel) configuration. According

to Eq. (7) a partial cancelation of the nonlinear energy shifts from contributions in the $++$ and $+ -$ channels is found in the co-linear (\parallel) configuration only. This, however, only slightly modifies the effective resonance frequencies (polariton dispersions) and thus slightly changes the optimum pump momentum and frequency. Most important for the stimulated amplification process is the difference in the polarization state configurations that can be seen in Eq. (8). Whereas for the co-linear (\parallel) configuration the sum of the scattering matrices in the $++$ and $+ -$ polarization state channels determines the strength of the phase-conjugate feedback driving the instability, for the cross-linear (\perp) configuration the difference of the two is relevant. Compared to the results without correlations in the $+ -$ channel, the difference in sign in the real parts of these two contributions [cf. Fig. 1(b)] leads to strong cancelation in Eq. (8) for the co-linear configuration and to strong enhancement in the cross-linear configuration. As previously pointed out in Ref. 18 this leads to an imbalance in the pairwise scattering of polaritons into the probe and FWM directions with polarization parallel or perpendicular to the pump. From our results we conclude that this does not necessarily lead to an overall rotation of the vectorial polarization state by 90° in contrast to the conclusions in Ref. 21. Based on our explicit treatment of the bound biexciton, we also find that in the studied system the scattering matrix element \mathcal{T}^{+-} that drives the amplification process by scattering of polaritons with opposite spins is not small compared to \mathcal{T}^{++} . We note that this is in contrast to the case reported in Ref. 19. Our results indicate that in the cw regime for a linearly polarized pump and close to threshold, spontaneous fluctuations preferably grow in the cross-linear polarization configuration. This is in agreement with recent observations for a slightly different system and excitation geometry.²⁴

The above discussion has a very general character. The actual cancelation of the different contributions in Eqs. (6)-(8) depends quantitatively on parameters such as the coupling strength of the cavity-modes to the excitonic polarization amplitudes. The general trend follows from the frequency dependence of the two-exciton scattering matrices as shown in Fig. 1(b): The stronger the cavity-mode exciton coupling (shifting the “magic angle” to larger negative detuning) the less pronounced the role of \mathcal{T}^{+-} will be. However, especially close to threshold even a small difference in growth rates can be crucial, and in this regime even a small \mathcal{T}^{+-} contribution can play a major role for the analysis of vectorial polarization state rotations. Although for the system studied here it was found to be almost insignificant, the overall role of the TE-TM cavity-mode splitting can depend on parameters and excitation conditions, too. Furthermore the importance of a TE-TM cavity-mode splitting can be different in other systems such as the quasi-one-dimensional microcavity system studied in Ref. 20.

Although not relevant for the amplification of polaritons on the LPB, we finally note that Figs. 3 to 5 show

strong pump-induced EID for excitation on the UPB. Although the two-exciton scattering matrices evaluated in the 1s approximation are not quantitatively accurate in this energy region, even in a theory including only coherent excitations this additional EID would likely inhibit the observation of any instability in the UPB (previously discussed, e.g., in Ref. 43) in analogy to the situation for positive pump detuning in a single QW¹¹.

V. CONCLUSIONS

Based on a microscopic many-particle theory we have investigated the influence of excitonic correlations on the vectorial polarization state characteristics of the parametric amplification of polaritons in semiconductor microcavities. By means of a linear stability analysis it has been analyzed how a linearly polarized pump can induce a polarization state anisotropy in an otherwise perfectly isotropic microcavity system. For the discussion of this effect we take advantage of our theoretical approach which – in contrast to previous models^{16,17,18,19} – is based on microscopically calculated exciton-exciton scattering matrix elements. Accounting for all coherent correlations between two excitons, these matrix elements determine the nonlinear cavity-polariton dynamics in the probe and FWM directions in the amplification regime.

A previous study¹⁰ found that excitonic correlations weaken the polariton amplification for co-circular pump-probe excitation. We confirm these findings and additionally investigate the effects of correlations on the polariton amplification in linearly polarized pump-probe configurations. We find that scattering contributions of the excitonic components of polaritons with opposite spins can strongly diminish the driving force for the amplification, the phase-conjugate coupling, in the co-linear (TE-TE or TM-TM) pump-probe polarization configuration and strongly enhance it in the cross-linear (TE-TM or TM-TE) configuration. In the spectral region where instability occurs the scattering of polaritons with opposite spins is dominated by the virtual formation of bound biexcitons.

In or close to the unstable regime this polarization state anisotropy has the potential to alter the polarization state of an amplified probe pulse compared to the incident probe. If the incoming probe has both components polarized parallel and perpendicular to the pump’s polarization state, in general the maximum growth rate for these two components over time is not the same. Then after a certain growth period the amplification of these two polarization state components will be different, and hence the vectorial polarization state of the outgoing probe is rotated compared to the incoming one’s. Since the probe component polarized perpendicular to the pump’s polarization vector grows faster over time than the parallel component, the probe is always rotated toward the “preferred” cross-linear configuration. However, the overall rotation in the vectorial polarization state depends on

both the duration of amplification and the difference in the growth rates in the two polarization state channels.

Finally, we note that in a situation where steady-state pump excitation brings only the cross-linear configuration above the unstable amplification threshold, without an incoming probe, only spontaneous fluctuations in the cross-linear polarization state channel will be amplified and thus observed as a finite signal in probe and FWM direction.

Acknowledgments

This work has been financially supported by ONR, DARPA, JSOP. S. Schumacher gratefully acknowledges financial support by the Deutsche Forschungsgemeinschaft (DFG, project No. SCHU 1980/3-1).

APPENDIX A: NONLINEAR PUMP EQUATION

The linear stability analysis of probe and FWM dynamics in Sec. III is done for monochromatic cw pump excitation. The stationary pump field inside the cavity, $E_{\mathbf{k}_p}^{\text{TM}}$, and pump-induced polarization amplitude in the QW, $p_{\mathbf{k}_p}^{\text{X}}$, which enter the matrix M in Eq. (3) are needed to analyze the probe and FWM dynamics. In this work we have considered pump excitation with a linearly polarized pump in the TM or TE cavity mode with in-plane momentum \mathbf{k}_p along a certain axis, here, without loss of generality the x axis, i.e., $\varphi_{\mathbf{k}_p} = 0$. Seeking a steady-state solution for the pump-induced polarization amplitude $p_{\mathbf{k}_p}^{\text{X}}$ we use the ansatz $E_{\mathbf{k}_p,\text{inc}}^{\text{TM}} = \tilde{E}_{\mathbf{k}_p,\text{inc}}^{\text{TM}} e^{-i\omega_p t}$, $E_{\mathbf{k}_p}^{\text{TM}} = \tilde{E}_{\mathbf{k}_p}^{\text{TM}} e^{-i\omega_p t}$ for the incoming pump field and the field in the excited cavity mode, respectively, and $p_{\mathbf{k}_p}^{\text{X}} = \tilde{p}_{\mathbf{k}_p}^{\text{X}} e^{-i\omega_p t}$ for the polarization amplitude, with $\dot{\tilde{E}}_{\mathbf{k}_p,\text{inc}}^{\text{TM}} = \dot{\tilde{E}}_{\mathbf{k}_p}^{\text{TM}} = \dot{\tilde{p}}_{\mathbf{k}_p}^{\text{X}} = 0$. Then from Eq. (1) it follows that the electric field in the cavity mode for in-plane momentum \mathbf{k}_p is given by:

$$\tilde{E}_{\mathbf{k}_p}^{\text{TM}} = \frac{-V_{k_p}^{\text{TM}} \tilde{p}_{\mathbf{k}_p}^{\text{X}} + i\hbar t_c \tilde{E}_{\mathbf{k}_p,\text{inc}}^{\text{TM}}}{\hbar\omega_p - \hbar\omega_{k_p}^{\text{TM}} + i\gamma_c}. \quad (\text{A1})$$

For unidirectional light propagation, i.e., by removing all sums in Eq. (2), taking all field and polarization amplitude variables at momentum \mathbf{k}_p , and replacing the pump field by Eq. (A1), a cubic equation of the form

$$0 = a_0 + a_1 |\tilde{p}_{\mathbf{k}_p}^{\text{X}}|^2 + a_2 |\tilde{p}_{\mathbf{k}_p}^{\text{X}}|^4 + |\tilde{p}_{\mathbf{k}_p}^{\text{X}}|^6 \quad (\text{A2})$$

can be derived. This equation determines the monochromatic solutions for each pump frequency ω_p and incoming pump intensity ($\sim |E_{\mathbf{k}_p,\text{inc}}^{\text{TM}}|^2$). The coefficients in

Eq. (A2) are

$$a_0 = -\frac{1}{|\tilde{T}|^2} \frac{\hbar^2 t_c^2 V_{k_p}^{\text{TM}2} |\tilde{E}_{\mathbf{k}_p,\text{inc}}^{\text{TM}}|^2}{(\hbar\omega_p - \hbar\omega_{k_p}^{\text{TM}})^2 + \gamma_c^2},$$

$$a_1 = \frac{1}{|\tilde{T}|^2} \left(|\tilde{\varepsilon}|^2 + \frac{2\hbar^2 t_c^2 V_{k_p}^{\text{TM}2} \tilde{A} |\tilde{E}_{\mathbf{k}_p,\text{inc}}^{\text{TM}}|^2}{(\hbar\omega_p - \hbar\omega_{k_p}^{\text{TM}})^2 + \gamma_c^2} \right),$$

and

$$a_2 = \frac{2}{|\tilde{T}|^2} \left(\text{Re}\{\tilde{\varepsilon}\} \text{Re}\{\tilde{T}\} + \text{Im}\{\tilde{\varepsilon}\} \text{Im}\{\tilde{T}\} - \frac{\hbar^2 t_c^2 V_{k_p}^{\text{TM}2} \tilde{A}^2 |\tilde{E}_{\mathbf{k}_p,\text{inc}}^{\text{TM}}|^2}{(\hbar\omega_p - \hbar\omega_{k_p}^{\text{TM}})^2 + \gamma_c^2} \right),$$

with the definitions

$$\tilde{\varepsilon} = \hbar\omega_{k_p}^{\text{X}} - \hbar\omega_p - i\gamma_x + \frac{V_{k_p}^{\text{TM}2}}{\hbar\omega_p - \hbar\omega_{k_p}^{\text{TM}} + i\gamma_c},$$

$$\tilde{T} = \frac{1}{2} (\tilde{T}^{++} + \tilde{T}^{+-}) - \frac{V_{k_p}^{\text{TM}2} \tilde{A}}{\hbar\omega_p - \hbar\omega_{k_p}^{\text{TM}} + i\gamma_c}.$$

Being a cubic equation in $|\tilde{p}_{\mathbf{k}_p}^{\text{X}}|^2$, depending on the coefficients a_0, a_1, a_2 , Eq. (A2) can have either one or three real-valued solutions. These solutions are given, e.g., in Ref. 44.

Equation (A2) only determines the magnitude of the pump-induced polarization amplitude $|\tilde{p}_{\mathbf{k}_p}^{\text{X}}|$ and contains no information about the different phases of the polarization amplitude and the incoming field. We define a phase ϕ according to $\tilde{E}_{\mathbf{k}_p,\text{inc}}^{\text{TM}} \cdot \tilde{p}_{\mathbf{k}_p}^{\text{X}} = |\tilde{E}_{\mathbf{k}_p,\text{inc}}^{\text{TM}}| |\tilde{p}_{\mathbf{k}_p}^{\text{X}}| e^{i\phi}$. This phase ϕ is required to determine the field in the cavity mode from Eq. (A1) that is coupled to the polarization amplitude. The field enters the linear stability analysis via the PSF terms in M . If we choose the solution of Eq. (A2) to be real, $\tilde{p}_{\mathbf{k}_p}^{\text{X}} = |\tilde{p}_{\mathbf{k}_p}^{\text{X}}|$, then the incoming field inducing this polarization amplitude is $\tilde{E}_{\mathbf{k}_p,\text{inc}}^{\text{TM}} = |\tilde{E}_{\mathbf{k}_p,\text{inc}}^{\text{TM}}| e^{i\phi}$. The phase of the incoming field can be obtained from Eq. (2) and is given by

$$e^{i\phi} = \frac{(\tilde{\varepsilon} |\tilde{p}_{\mathbf{k}_p}^{\text{X}}| + \tilde{T} |\tilde{p}_{\mathbf{k}_p}^{\text{X}}|^3) (\hbar\omega_p - \hbar\omega_{k_p}^{\text{TM}} + i\gamma_c)}{i\hbar t_c V_{k_p}^{\text{TM}} (1 - \tilde{A} |\tilde{p}_{\mathbf{k}_p}^{\text{X}}|^2) |\tilde{E}_{\mathbf{k}_p,\text{inc}}^{\text{TM}}|},$$

which then also determines the phase of the field in the cavity mode given by Eq. (A1).

- ¹ P. G. Savvidis, J. J. Baumberg, R. M. Stevenson, M. S. Skolnick, D. M. Whittaker, and J. S. Roberts, *Phys. Rev. Lett.* **84**, 1547 (2000).
- ² R. Huang, F. Tassone, and Y. Yamamoto, *Phys. Rev. B* **61**, R7854 (2000).
- ³ C. Ciuti, P. Schwendimann, B. Deveaud, and A. Quattropani, *Phys. Rev. B* **62**, R4825 (2000).
- ⁴ R. M. Stevenson, V. N. Astratov, M. S. Skolnick, D. M. Whittaker, M. Eman-Ismail, A. I. Tartakovskii, P. G. Savvidis, J. J. Baumberg, and J. S. Roberts, *Phys. Rev. Lett.* **85**, 3680 (2000).
- ⁵ M. Saba, C. Ciuti, J. Bloch, V. Thierry-Mieg, R. Andre, Le Si Dang, S. Kundermann, A. Mura, G. Bongiovanni, J. L. Staehli, et al., *Nature* **414**, 731 (2001).
- ⁶ D. M. Whittaker, *Phys. Rev. B* **63**, 193305 (2001).
- ⁷ C. Ciuti, P. Schwendimann, and A. Quattropani, *Semicond. Sci. Technol.* **18**, 279 (2003).
- ⁸ J. J. Baumberg and P. G. Lagoudakis, *Phys. Stat. Sol. (b)* **242**, 2210 (2005).
- ⁹ J. Keeling, F. M. Marchetti, M. H. Szymanska, and P. B. Littlewood, *Semicond. Sci. Technol.* **22**, R1 (2007).
- ¹⁰ S. Savasta, O. Di Stefano, and R. Girlanda, *Phys. Rev. Lett.* **90**, 096403 (2003).
- ¹¹ S. Schumacher, N. H. Kwong, R. Binder, and A. L. Smirl, submitted, arXiv.org:cond-mat/0708.0442v1 (2006).
- ¹² S. Savasta, O. Di Stefano, and R. Girlanda, *Semicond. Sci. Technol.* **18**, S294 (2003).
- ¹³ J. A. Bolger, A. E. Paul, and A. L. Smirl, *Phys. Rev. B* **54**, 11666 (1996).
- ¹⁴ C. Ramkumar, T. Aoki, R. Shimano, Y. P. Svirko, T. Kise, T. Someya, H. Sakaki, and M. Kuwata-Gonokami, *J. Phys. Soc. J.* **69**, 2439 (2000).
- ¹⁵ P. G. Lagoudakis, P. G. Savvidis, J. J. Baumberg, D. M. Whittaker, P. R. Eastham, M. S. Skolnick, and J. S. Roberts, *Phys. Rev. B* **65**, 161310(R) (2002).
- ¹⁶ A. Kavokin, P. G. Lagoudakis, G. Malpuech, and J. J. Baumberg, *Phys. Rev. B* **67**, 195321 (2003).
- ¹⁷ P. R. Eastham and D. M. Whittaker, *Phys. Rev. B* **68**, 075324 (2003).
- ¹⁸ P. Renucci, T. Amand, X. Marie, P. Senellart, J. Bloch, B. Sermage, and K. V. Kavokin, *Phys. Rev. B* **72**, 075317 (2005).
- ¹⁹ K. V. Kavokin, P. Renucci, T. Amand, X. Marie, P. Senellart, J. Bloch, and B. Sermage, *Phys. Stat. Sol. (c)* **2**, 763 (2005).
- ²⁰ G. Dasbach, C. Diederichs, J. Tignon, C. Ciuti, Ph. Rousignol, C. Delalande, M. Bayer, and A. Forchel, *Phys. Rev. B* **71**, 161308(R) (2005).
- ²¹ D. N. Krizhanovskii, D. Sanvitto, I. A. Shelykh, M. M. Glazov, G. Malpuech, D. D. Solnyshkov, A. Kavokin, S. Ceccarelli, M. S. Skolnick, and J. S. Roberts, *Phys. Rev. B* **73**, 073303 (2006).
- ²² G. Panzarini, L. C. Andreani, A. Armitage, D. Baxter, M. S. Skolnick, V. N. Astranov, J. S. Roberts, A. V. Kavokin, M. R. Vladimirova, and M. A. Kaliteevski, *Phys. Rev. B* **59**, 5082 (1999).
- ²³ K. V. Kavokin, I. A. Shelykh, A. V. Kavokin, G. Malpuech, and P. Bigenwald, *Phys. Rev. Lett.* **92**, 017401 (2004).
- ²⁴ M. Romanelli, C. Leyder, J. Ph. Karr, E. Giacobino, and A. Bramati, *Phys. Rev. Lett.* **98**, 106401 (2007).
- ²⁵ R. Takayama, N. H. Kwong, I. Romyantsev, M. Kuwata-Gonokami, and R. Binder, *Eur. Phys. J. B* **25**, 445 (2002).
- ²⁶ V. M. Axt and A. Stahl, *Z. Phys. B* **93**, 195 (1994).
- ²⁷ T. Östreich, K. Schönhammer, and L. J. Sham, *Phys. Rev. Lett.* **74**, 4698 (1995).
- ²⁸ N. H. Kwong, R. Takayama, I. Romyantsev, M. Kuwata-Gonokami, and R. Binder, *Phys. Rev. B* **64**, 045316 (2001).
- ²⁹ N. H. Kwong, R. Takayama, I. Romyantsev, M. Kuwata-Gonokami, and R. Binder, *Phys. Rev. Lett.* **87**, 027402 (2001).
- ³⁰ T. Östreich and L. J. Sham, *Phys. Rev. Lett.* **83**, 3510 (1999).
- ³¹ M. Buck, L. Wischmeier, S. Schumacher, G. Czycholl, F. Jahnke, T. Voss, I. Rückmann, and J. Gutowski, *Eur. Phys. J. B* **42**, 175 (2004).
- ³² S. Schumacher, G. Czycholl, F. Jahnke, I. Kudyk, L. Wischmeier, I. Rückmann, T. Voss, J. Gutowski, A. Gust, and D. Hommel, *Phys. Rev. B* **72**, 081308(R) (2005).
- ³³ The background refractive index, effective electron mass, and effective hole mass are $n_{bg} = 3.61$, $m_e = 0.067 m_0$, and $m_h = 0.1 m_0$, respectively. The corresponding exciton binding energy is $E_b^x \approx 13$ meV and the bulk Bohr-radius is $a_0^x \approx 170 \text{ \AA}$. For the evaluation of the theory also $\varepsilon_k^x = 1.4965$ eV, $A^{\text{PSF}} = 4a_0^x \sqrt{2\pi}/7$, $E_b^{xx} \approx 1.84$ meV, and $\gamma_x = 0.25$ meV are required. The cavity parameters are $\gamma_c = 0.25$ meV, and $V_0^{\text{TM}} = 5.2$ meV.
- ³⁴ M. E. Donovan, A. Schülzgen, J. Lee, P.-A. Blanche, N. Peyghambarian, G. Khitrova, H. M. Gibbs, I. Romyantsev, N. H. Kwong, R. Takayama, et al., *Phys. Rev. Lett.* **87**, 237402 (2001).
- ³⁵ S. Savasta and R. Girlanda, *Phys. Rev. Lett.* **77**, 4736 (1996).
- ³⁶ V. Savona, F. Tassone, C. Piermarocchi, A. Quattropani, and P. Schwendimann, *Phys. Rev. B* **53**, 13051 (1996).
- ³⁷ Alternatively to the chosen notation, the excitonic polarization can also be expressed in terms of longitudinal and transverse components with respect to \mathbf{k} . This way the “artificial” choice of a fixed coordinate system, like in our case the X-Y basis, can be avoided. However, then the appearance of angular dependencies containing the azimuthal angle relative to \mathbf{k} are inherent in the nonlinear terms coupling polarizations and fields with different in-plane momenta.
- ³⁸ N. H. Kwong, S. Schumacher, and R. Binder, to be submitted (2007).
- ³⁹ P. Borri, W. Langbein, U. Woggon, J. R. Jensen, and J. M. Hvam, *Phys. Rev. B* **62**, R7763 (2000).
- ⁴⁰ M. Kuwata-Gonokami, S. Inouye, H. Suzuura, M. Shirane, R. Shimano, T. Someya, and H. Sakaki, *Phys. Rev. Lett.* **79**, 1341 (1997).
- ⁴¹ N. A. Gippius, S. G. Tikhodeev, V. D. Kulakovskii, D. N. Krizhanovskii, and A. I. Tartakovskii, *Europhys. Lett.* **67**, 997 (2004).
- ⁴² M. Wouters and I. Carusotto, *Phys. Rev. B* **75**, 075332 (2007).
- ⁴³ C. Ciuti, *Phys. Rev. B* **69**, 245304 (2004).
- ⁴⁴ M. Abramowitz and I. A. Stegun, *Handbook of mathematical functions with formulas, graphs, and mathematical tables* (U.S. Govt. Print. Off., Washington, 1972).